Structural insights into TSC complex assembly and GAP activity on Rheb

Huirong Yang
Shanghai Medical College of Fudan University
Zishuo Yu
Shanghai Medical College of Fudan University
Xizi Chen
Shanghai Medical College of Fudan University
Jiabei Li
Shanghai Medical College of Fudan University
Ningning Li
Peking University https://orcid.org/0000-0001-8601-5171
Jiaxuan Cheng
Peking University https://orcid.org/0000-0001-9210-746X
Ning Gao
Peking University https://orcid.org/0000-0003-3067-9993
Hai-Xin Yuan
Fudan University https://orcid.org/0000-0002-1624-3934
Dan Ye
Fudan University
Kun-Liang Guan
University of California San Diego https://orcid.org/0000-0003-1892-0174
Yanhui Xu (xuyh@fudan.edu.cn)
Fudan University https://orcid.org/0000-0002-1408-5178

Article

Keywords: Tuberous sclerosis complex, GAP activity, Rheb

Posted Date: July 7th, 2020

DOI: https://doi.org/10.21203/rs.3.rs-36453/v1

Version of Record: A version of this preprint was published at Nature Communications on January 12th, 2021. See the published version at https://doi.org/10.1038/s41467-020-20522-4.

Abstract

Tuberous sclerosis complex (TSC) integrates upstream stimuli and regulates cell growth by controlling the activity of mTORC1. TSC functions as a GTPase-activating protein (GAP) towards small GTPase Rheb and inhibits Rheb-mediated activation of mTORC1. Mutations in TSC genes cause tuberous sclerosis. In this study, the near-atomic resolution structure of human TSC complex reveals an arch-shaped architecture, with a 2:2:1 stoichiometry of TSC1, TSC2, and TBC1D7. This asymmetric complex consists of two interweaved TSC1 coiled-coil and one TBC1D7 that spans over the tail-to-tail TSC2 dimer. The two TSC2 GAP domains are symmetrically cradled within the core module formed by TSC2 dimerization domain and central coiled-coil of TSC1. Structural and biochemical analyses reveal TSC2 GAP-Rheb complimentary interactions and suggest a catalytic mechanism, by which an asparagine thumb (N1643) stabilizes γ-phosphate of GTP and accelerate GTP hydrolysis of Rheb. Our study reveals mechanisms of TSC assembly and GAP activity.

Introduction

The mechanistic target of rapamycin complex 1 (mTORC1) is a master regulator of cell growth by phosphorylating a variety of substrates, as exemplified by ribosomal S6 kinase 1 (S6K1) and eukaryote initiation factor 4E binding protein (4EBP)[1,2]. As a well-known tumor suppressor, the tuberous sclerosis complex (TSC) integrates cues of growth factors, energy status and various stress to maintain Rheb in GDP-bound state, and therefore keeps mTORC1 in check to limit undesirable cell growth[2–5]. The TSC acts as a GTPase-activating protein (GAP) towards a small G-protein Ras homolog enriched in brain (Rheb) required for mTORC1 activation[6]. In GTP-bound state, Rheb directly binds to and activates mTORC1[7–11].

The TSC complex consists of Tuberous Sclerosis Complex 1 (TSC1), Tuberous Sclerosis Complex 2 (TSC2) and an auxiliary subunit Tre2-Bub2-Cdc16-1 domain family member 7 (TBC1D7)[4,5]. Mutations of *TSC1* or *TSC2* genes cause tuberous sclerosis, an autosomal dominant genetic disease characterized by the development of histologically diverse hamartomas or benign tumors, including skin, brain, and kidneys[5,12]. TSC patients are frequently associated with severe neurological manifestations, including epilepsy, intellectual disability and autism[5,13]. Although the functions of TSC have been extensively studied for decades, there are only a few structures of isolated domains, including TSC1 peptide bound to TBC1D7[3,14], N-terminal domains of yeast TSC1[15] and TSC2 (*Chaetomium thermophilum*)[16]. The lack of TSC complex structure has hampered understanding the mechanisms for complex assembly, GAP activity, and disease correlation.

Here we present the first cryo-EM structure of human TSC complex and elaborate on its characteristic assembly and GAP function. Our structure also provides a framework for understanding the regulation of TSC function in mTORC1 pathway and its pathological significance.

Results

Structure determination. To obtain TSC structure, we overexpressed human TSC1, TSC2, and TBC1D7 in Expi293F cells and purified the complex to homogeneity (Supplementary Fig. 1a). The purified TSC complex showed relatively weak in vitro GAP activity against Rheb, consistent with the known poor in vitro activity[8,17] (Supplementary Fig. 1b). The structure was determined by cryo-EM single particle reconstruction and the cryo-EM map was refined to an overall resolution of 4.4 Å (Fig. 1b). The core and two wings were locally refined to 3.6 Å, 3.9 Å, and 4.1 Å resolution, respectively (Supplementary Figs. 2 and 3). The majority of structural model was unambiguously built *ab initio* aided by the structure of TSC1 fragment bound to TBC1D7[14] and secondary structure analyses (Table 1 and Supplementary Movies 1–4). The TSC1 (residues 746–971), TSC2 (residues 127–1732), and TBC1D7 (residues 21–287) were modeled, in which a few regions were built using poly alanine due to the weak cryo-EM density (Supplementary Fig. 4).

Table 1
Statistics of cryo-EM data collection, refinement and validation statistics.

	TSC
Data collection and processing	
Magnification	105,000x
Voltage (kV)	300
Electron exposure (e–/Å^2)	50
Defocus range (μm)	1.0 to 3.5
Pixel size (Å)	1.356
Symmetry imposed	C1
Initial particle images (no.)	1,528,982
Final particle images (no.)	131,022
Map resolution (Å)	4.4
Consensus reconstruction	4.1
Focus wing-a reconstruction	3.6
Focus core reconstruction	3.9
Focus wing-b reconstruction	0.143
FSC threshold	
Map resolution range (Å)	4.0–20.0
Consensus reconstruction	4.0–20.0
Focus wing-a reconstruction	3.0–10.0
Focus core reconstruction	3.0–10.0
Focus wing-b reconstruction	
Refinement	
Initial model used (PDB code)	5EJC
Model resolution (Å)	4.5
FSC threshold	0.5
Model resolution range (Å)	4.0-4.5
Map sharpening *B* factor (Å^2)	-129.92

	TSC
Model composition	23934
Non-hydrogen atoms	3089
Protein residues	0
Ligands	
B factors (Å^2)	141.96
Protein	—
Ligand	
R.m.s. deviations	0.004
Bond lengths (Å)	0.673
Bond angles (°)	
Validation	2.42
MolProbity score	24.52
Clashscore	0.12
Poor rotamers (%)	
Ramachandran plot	90.30
Favored (%)	9.70
Allowed (%)	0.00
Disallowed (%)	

Overall structure of human TSC. The complex consists of a central core and two wings (termed wing-a and wing-b) and the overall structure exhibits an elongated arch-shaped fold with approximate dimensions of ~ 390 × 133 × 88 Å^3 (Fig. 1b). TSC1, TSC2, and TBC1D7 assemble the TSC complex with a 2:2:1 stoichiometry, generating an asymmetric modular organization. Although isolated domains adopt similar folds, the two TSC1 (termed TSC1a/1b) and two TSC2 (TSC2a/2b) reveal distinct conformations, respectively (Supplementary Fig. 5). The two TSC2 molecules form a pseudo-symmetric dimer through tail-to-tail interactions. The coiled-coil domains (CCs, residues 746–971) of TSC1a and TSC1b interwind in parallel and form an extended two-helix bundle (Fig. 1c and Supplementary Fig. 6a-d), which makes multiple contacts with TSC2 dimer and stabilizes the overall conformation of the complex. This parallel dimerization of TSC1 leads to an asymmetric formation of TSC1-TSC2 tetramer and recruitment of a single TBC1D7 molecule, generating a unique and characteristic modular organization (Fig. 1b and Supplementary Fig. 5f-g).

Each TSC2 consists of a HEAT repeat domain (HEAT), a dimerization domain (DD), followed by a C-terminal GAP catalytic domain (GAP) (Fig. 1a, b, d). The N-terminal twelve HEAT repeats (wing HEAT, wHEAT) flank out of the central core and are stabilized by TSC1. The following six HEAT repeats (core HEAT, cHEAT) associate with and are stabilized by the central GAP and DD domains. The cHEAT-DD-GAP of the two TSC2 molecules adopt pseudo-symmetric fold whereas the two wHEAT domains adopt distinct conformations due to differently associated TSC1 (Supplementary Fig. 5). TSC2a and TSC2b bind the N-terminal (N-CC) and C-terminal (C-CC) halves of the TSC1 CC dimer, respectively (Fig. 1b).

The TBC1D7 associates with the C-terminal helices (residues 937–971) of TSC1a/1b but has no direct contact with TSC2. The TBC1D7-TSC1a/1b module adopts a similar fold to the human TSC1-TBC1D7 crystal structure[14] (Supplementary Fig. 6e), and is positioned far away from the central core, consistent with its auxiliary role in TSC assembly and function[4]. The observation agrees with immunoprecipitation results showing that TBC1D7 binds TSC1 but not TSC2 (Supplementary Fig. 6f).

TSC1 structure and its interaction with TSC2. The two CC domains of TSC1a and TSC1b are paired in parallel and form a two-turn left-handed supercoil (Fig. 1c). The pairwise coiled-coil involves extensive intermolecular contacts. The TSC1 homodimer interface is enriched in nonpolar residues, which make extensive hydrophobic contacts to support a stable TSC1 dimerization and its scaffolding function (Supplementary Fig. 6a-d). Sequence alignment indicates that the coiled-coil region of TSC1 is highly conserved across eukaryotic species, suggesting an evolutionarily conserved dimeric coiled-coil conformation (Supplementary Fig. 4b).

The TSC1 CC dimer adopts an arch-shaped architecture and packs against the ridge of TSC2 dimer (Figs. 1b, 2a). The CC dimer makes four major contacts with TSC2. (1) The central region of TSC1a (residues 800–890) sits on a “saddle” formed by TSC2 DD dimer (Fig. 2b, c). (2) The TSC1a-N-CC (residues 746–795) packs against the ridge of repeats HEAT7-HEAT12 of TSC2a (Fig. 2d). (3) The C-CC (residues 890–936) dimer of TSC1 packs against the ridge of the repeats HEAT8-HEAT12 of TSC2b (Fig. 2e). (4) The TSC1a-C-CC (residues 937–971) packs against the ridge of repeats HEAT3-HEAT7 of TSC2b (Fig. 2f), confirmed the known interaction between the N-terminus of TSC2 (residues 1-418) and TSC1[16,18,19]. Consistent with the asymmetric complex formation, TSC1a plays a major role in binding TSC2 dimer.

Another asymmetric feature of the complex exists around the end of wing-a module. The cryo-EM map reveals repetitive helical region covering the N-terminal HEAT repeats of TSC2a but not TSC2b. This region is likely derived from the predicted N-terminal HEAT repeat domain of TSC1 (Fig. 1b and Supplementary Fig. 4b)[15]. Other TSC1 regions were invisible in our cryo-EM map due to flexibility, suggesting a nonessential role in TSC complex assembly. In our immunoprecipitation assay, the full-length and CC of TSC1 shows comparable binding to TSC2 (Supplementary Fig. 6g), consistent with the maintenance of TSC1-TSC2 upon deletion of TSC1 several N-terminal fragments[20].

Domain organization and dimerization of TSC2. The TSC2 monomer adopts a seahorse-shaped conformation, in which the wHEAT (HEAT1 to HEAT12) and cHEAT (HEAT13-HEAT18) together adopt a right-handed super helical fold (Fig. 1d). The isolated cHEAT and wHEAT domains adopt almost identical conformations, respectively, in the two TSC molecules. However, the whole HEAT domain of TSC2b tends to be more extended than that of TSC2a (Supplementary Fig. 5e-g). The two HEAT domains bind the TSC1 dimer in a distinct manner, suggesting that different features of N- and C-terminal portions of TSC1 CC dimer lead to distinct conformation of the two TSC2 molecules (Supplementary Fig. 5f).

The cHEAT-DD-GAP parts of two TSC2 molecules form an almost symmetrical core of the complex and the dimerization is mediated by two stably associated DD domains (Fig. 2a-c and Supplementary Fig. 5c-e). Each DD domain consists of a four-stranded antiparallel β-sheet (Dβ1-Dβ4) and five flanking α-helices (Dα1-Dα5) (Fig. 2c). The two β-sheets together form a saddle-shaped eight-stranded β-sheet. The Dα5 helix (residues 1472–1483) packs against the concave surface of the saddle and binds the other TSC2 molecule on HEAT18 and the following loop (residues 1024–1038) (Fig. 2a and Supplementary Fig. 7). The loop preceding helix Dα4 inserts into a hydrophobic pocket of the other TSC2 molecule located in a three-way junction formed by the cHEAT, DD, and GAP domains (Fig. 2a). The TSC2 dimerization is further supported by DD helices of the two TSC2 molecules, which sandwich the TSC1a CC domain. Around this region, the TSC2 dimer interface (~ 2805Å^2) is larger than TSC1-TSC2 interface (~ 1761Å^2), suggesting that TSC2 forms homodimer independent of TSC1 and the TSC2 dimer is required for generating a stable TSC1-TSC2 tetramer[21].

The TSC2 GAP structure and its positioning in TSC complex. The two GAP catalytic domains are symmetrically cradled within the central core module and each GAP adopts a characteristic mixed α/β fold (Figs. 1b and 3a). A central seven-stranded β-sheet is stabilized by a long α helix (Gα5) from the concave side. The helix Gα3 (catalytic helix) and two loops (L1 and L2) pack against the convex surface of the β-sheet. Three intermodular contacts involve positioning of each GAP domain (Fig. 3a and Supplementary Fig. 8). (1) Two parallel α helices (GαN and GαC) form a GAP extension, which protrudes out of the catalytic core and binds the edge of the β-sheet of the DD domain and repeats HEAT17-HEAT18 (Supplementary Fig. 8b). (2) The helix Gα5, strand Gβ7 and its preceding loop, together pack against the concave surface of repeats HEAT13 to HEAT16 (Supplementary Fig. 8c). (3) The helix Gα1 (TSC2b) or Gα2 (TSC2a) and loop L1 bind TSC1 coiled-coil and the binding pattern is slightly different in two GAP domains. The GAP of TSC2a binds single CC (residues 800–830) of TSC1b whereas the GAP of TSC2b binds two CC strands (residues 860–895) of TSC1a/1b (Supplementary Fig. 8d). The lack of TSC1 largely decreased the GAP activity, indicating that TSC1 is required for assembly of fully active GAP domains in TSC complex (Supplementary Fig. 6h). The two GAP catalytic core adopt almost identical conformations and their catalytic pockets both open outwards, suggesting a similar manner of substrate recognition and catalysis (Fig. 2a and Supplementary Fig. 5d-e).

Catalytic mechanism of TSC2 GAP. The TSC2 GAP domain is highly conserved from yeast to human and shares considerable sequence homology to Rap1GAP (Supplementary Fig. 9a), suggesting that TSC2-stimulated GTP hydrolysis of Rheb follows the same mechanism as in Rap-Rap1GAP system[8,17,19]. To

investigate the mechanism of TSC2-stimulated GTP hydrolysis of Rheb, we superimposed TSC2 GAP structure and Rheb-GTP (PDB: 1XTS)[22] with Rap-Rap1GAP structure (PDB: 3BRW)[17] and the classical small G protein Ras-RasGAP (PDB: 1WQ1)[23] (Fig. 3b-d). Structural comparison confirms the predicted structural similarity between the GAP domains of TSC2 and Rap1GAP and reveals distinct fold of the associated domains, which may provide substrate specificity (Fig. 3b, c).

Previous structural and biochemical studies of small GTPases and their GAPs have proposed a generally conserved activation mechanism[24,25]. All the GAP domains provide positively charged residues, neutralize negative charges generated during phosphoryl transfer reactions, and thus accelerate GTP hydrolysis[24,25]. Ras-RasGAP represents the prototypic small GTPase-GAP system, in which a trans-arginine finger (R789 in RasGAP) and a cis-glutamine (Q61 in Ras) are critical for catalysis through stabilizing the γ-phosphate in the transition state[23,26] (Fig. 3e, f). The arginine finger is shared by GAPs of some other Ras superfamily members[25]. As a representative exception, Rap1-RapGAP lacks the arginine finger, but instead, has an asparagine thumb (N290 in Rap1GAP), which stabilizes γ-phosphate and is essential for GAP activity[17,27] (Fig. 3g-h).

Superimposition of Rheb[22] and TSC2 GAP domain structures to the Rap1-Rap1GAP complex structure[17] suggests that Rheb binds TSC2 GAP in a manner similar to that in Rap1-Rap1GAP (Fig. 3b, c). The catalytic helix (Gα3, K^{1638}RHLGN^{1643}) of TSC2 faces toward the catalytic cavity formed by the switch I, switch II, and P-loop of the superimposed Rheb (Fig. 3i-j). The switch I is conserved among the small G proteins (Supplementary Fig. 9b). Residue N1643 of TSC2 is similarly positioned to N290 of Rap1GAP, suggesting a shared asparagine thumb of the two GAP domains. As an equivalent of residue Y32 of Rap1 and Y32 in Ras, residue Y35 of Rheb is positioned close to N1643 and may facilitate GTP hydrolysis. The TSC2 catalytic helix is located relatively closer to the Rheb compared to that in Rap1-RapGAP structure, suggesting the helix might rotate back upon binding Rheb and allow the reaction to occur (Fig. 3g, i).

Other residues of the catalytic helix may support catalytic helix conformation (Fig. 3i-j). Residues K1638 and R1639 (equivalent to K285 and R286 of Rap1GAP) face toward the putative Rheb. Residues H1640 and L1641 (equivalent to H287 and I288 of Rap1GAP) face toward the core of TSC2 GAP. The conformational stability of the equivalent catalytic helix of RasGAP is essential for its activity[6,23], suggesting that these catalytic helix residues may also be required for GAP activity (Fig. 3e, g, i).

We performed cell-based assay to investigate the GAP activity of TSC complex by detecting the phosphorylation of S6K1 at T389, which is well-accepted to represent the level of Rheb in GTP-bound form and TSC2 GAP activity[8,28] (Fig. 3k). The co-transfection of TSC1 and TSC2 largely decreased the level of phosphorylated-S6K1, indicating a robust GAP activity in cells (Fig. 3k, lanes 1–3). Alanine substitutions of K1638 or R1639 and tuberous sclerosis-associated mutation of K1638 showed weak to moderate defect on GAP activity (Fig. 3k, lanes 4–6), whereas alanine substitutions or tuberous sclerosis-associated mutations of H1640, L1641, or N1643 on TSC2, largely impaired the GAP activity (Fig. 3k,

lanes 7–12), to a level comparable to that of lacking TSC complex (Fig. 3k, lane 2). The result is consistent with structural observation and supports the notion that TSC2 uses the asparagine thumb (N1643) to accelerate GTP hydrolysis of Rheb and residues K1638, H1640 and L1641 of the catalytic helix function in supporting the conformation of the asparagine thumb. These results are consistent with previous studies[10,29], in which residues K1638, H1640, N1643 are important for TSC2 GAP activity.

The Rheb recognition by TSC2 GAP domain. Structure superimposition suggests that Rheb is well-accommodated by the TSC2 GAP domain and has no clash with other domains. This putative Rheb-TSC2 binding pattern differs from that of Rap1-Rap1GAP and Ras-RasGAP due to characteristic features of TSC2 GAP, which may confer specificity toward Rheb. Besides the catalytic helix, the loops L1 and L2 are respectively positioned close to switch II and switch I of the superimposed Rheb, possibly generating two putative TSC2-Rheb contacts (Fig. 3b-j and Supplementary Fig. 8e). Previous study reported that L1594 and F1666 mutations decreased GAP activity[29]. Our GAP assay shows that Alanine substitutions or disease-associated mutations of L1 (L1594, L1597), L2 (Q1665, F1666), and F1645 impaired its GAP activity, confirming their supportive roles in substrate recognition and/or catalysis (Fig. 3l, lanes 13–14 and 8–11).

The structure reveals a characteristic helix pair formed by GαN (residues 1525–1536) and GαC (residues 1739–1754) of TSC2 that was not observed in other GAP-GTPase systems. The helix pair is positioned near the helices α2 (residue Q72) and α3 (residues D105 and M106) of the superimposed Rheb and likely supports TSC2-Rheb interactions (Fig. 3f, h, j). Mutations R1529A, L1533A, and double mutation R1529A/L1533A on GαN and R1749A on GαC led to moderate to severe decrease in TSC2 GAP activity, suggesting their critical roles in supporting TSC2-Rheb contacts (Fig. 3l, lanes 4–7 and 12). Previous study also showed that R1749Q mutation (equivalent to R1707 in the short isoform used in this work) decreased the GAP activity to some extent[19]. During our manuscript preparation, Hansmann et al[30] reported the crystal structure of TSC2 GAP domain, which consists of the central core but lacks the helix pair. The isolated GAP domain structure is similar to that in TSC complex and the proposed mechanism of GAP activity on Rheb is consistent with our independent studies.

Discussion

Mutations of *TSC* genes have been frequently observed in tuberous sclerosis and cancers and missense mutations occurred throughout the protein sequences[31] (Fig. 4a and Supplementary Fig. 4). Notably, most of cancer derived mutations in *TSC2* are enriched on the central core module, supporting the pathological significance of TSC complex in these diseases. Furthermore, the mutations in the wing modules are predominantly enriched on the ridges of HEAT domains of TSC2, consistent with their roles in mediating TSC1-TSC2 interactions and TSC conformational stability[19,32–36].

The surface electrostatic calculations of TSC2 structure reveals four predominant positively charged patches around the DD (D-patch) and GAP (G-patch) domains. The four patches are located on the bottom surface of the central core and close to the putative Rheb-binding pockets of the two GAP

domains, suggesting a regulatory role related to its GAP function (Fig. 4b, c). It is tempting to speculate that these positively charged patches may involve charge-charge interactions and associate with negatively charged phosphorylated residues and/or lipids.

It is well documented that residues S939, S981, and T1462 of TSC2 are phosphorylated by the AKT kinase and these modifications promote TSC2 translocation from lysosomal membrane to the cytosol via binding of 14-3-3 protein, and therefore inhibit GAP activity on Rheb and activate mTORC1[37,38]. Residues T1271 and S1387 are phosphorylated by the AMPK kinase under energy deficiency, which leads to activation of TSC and inhibition of mTOR activity[39]. The MK2 kinase phosphorylates S1210 and modulates its interaction with 14-3-3[40,41]. Although these residues were invisible due to the lack of corresponding cryo-EM density, their nearest modeled residues, S937, R1245, and G1494, are located around these positively charged patches (Fig. 4c), which may recruit and stabilize these abovementioned phosphorylated residues.

Inactivation of mTORC1 requires TSC2 lysosomal localization[42]. The size of typical lysosome ranges from 100 nm to 1000 nm[43]. The characteristic arch-shaped architecture of TSC spans ~ 40 nm, suggesting that TSC may packs against the surface of lysosome and fits the membrane curvature (Fig. 4d). It is well known that TSC2 is recruited to lysosome membrane through nonexclusive pathways, such as binding C181 farnesylated Rheb[44], Rag GTPases[45], and polycystin-1[46]. Structural superimposition indicates that the farnesylated Rheb has no clash with the positive patches of TSC, supporting its co-localization with TSC on lysosomal surface (Fig. 4b and Supplementary Fig. 8f). Lipid phosphorylation has been known to regulate membrane localization of proteins[47]. TSC complex may bind phosphorylated lipid on lysosome membrane via its positive patches through charge-charge interactions, providing an alternative approach for its lysosomal localization.

Methods

Reagents. Flag M2 affinity agarose gel was from Raygene; Mono Q and Superose 6 were from GE Healthcare; Polyethylenimine (PEI) was from polysciences (23966); HEK293 cells were from Invitrogen. Inc. and culture medium were from Sino Biological Inc. Antibodies against phosphorylated-S6K (Thr 389) was from Cell Signaling Technology; Flag-HRP (A8592) from Sigma, Horseradish peroxidase-labeled anti-mouse and anti-rabbit secondary antibodies was from AbMart.

Protein expression and purification. The ORFs of human TSC1, TSC2 and TBC1D7 were sub-cloned into three modified pCAG vectors. The three plasmids were co-transfected to suspension Expi293F cells using Polyethylenimine (PEI). After culture at 37 °C, 5% CO2 for 3 days, cells were collected and lysed in 50 mM HEPES (pH 7.4), 300 mM NaCl, 0.2% CHAPS, 5 mM $MgCL_2$, 5 mM ATP, 10 mM NaF and 3 mM DTT at 4 °C for 30 min, and the insoluble fraction was removed by centrifugation at 16,000 rpm for 30 min. Supernatants were incubated with FLAG-M2 monoclonal antibody-agarose for 4 hours and washed extensively. The fusion proteins (FLAG-tagged TSC1, Myc-tagged TSC2 and Myc-tagged TBC1D7) were digested using PreScission protease overnight and the eluted proteins were further purified using ion

exchange and gel filtration chromatography. The peak fractions were pooled for gradient fixation (Grafix)[48]. The gradient was generated from a 10% glycerol light solution [10% (v/v) glycerol, 300 mM NaCl, 25 mM HEPES (pH 7.4), 1 mM TCEP], and a 30% glycerol heavy solution [30% (v/v) glycerol, 300 mM NaCl, 25 mM HEPES (pH 7.4), 1 mM TCEP, and 0.1% (v/v) glutaraldehyde]. Centrifugation was performed at 38,000 r.p.m. in a SW41Ti swinging bucket rotor for 18 h at 4 °C using Beckman L-100XP. Subsequently, peak fractions were collected and quenched with 100 mM Tris-HCl (pH 8.0). The cross-linked TSC complex was concentrated and dialyzed to 0.5 mg/ml for Cryo-EM grids.

Sample preparation. For negative staining EM grids preparation, 5 μL of TSC complex sample was applied onto glow-discharged copper grids supported by a continuous thin layer of carbon film for 60 s before negatively stained by 2% (w/v) uranyl formate solution at room temperature. The grids were prepared in the Ar/O_2 mixture for 15 s using a Gatan 950 Solarus plasma cleaning system with a power of 35W. The negatively stained grids were loaded onto a Thermo Fisher Scientific Talos L120C microscope equipped with a Ceta CCD camera and operating at 120 kV at a nominal magnification of 92,000 x, corresponding to a pixel size of 1.58 Å on the specimen.

For cryo-EM grids preparation, 4 μL of the sample at a concentration of ~ 0.5 mg/mL TSC complex was applied to freshly glow-discharged Quantifoil R1.2/1.3 holey carbon grids. After incubation of 5 s at a temperature of 4 °C and a humidity of 100%, the grids were blotted for 4 ~ 6 s in a Thermo Fisher Scientific Vitrobot Mark IV and plunge-frozen in liquid ethane at liquid nitrogen temperature. The grids were prepared in the H_2/O_2 mixture for 60 s using a Gatan 950 Solarus plasma cleaning system with a power of 5W. The ø 55/20 mm blotting paper is made by TED PELLA used for plunge freezing.

Data collection. The cryo-EM grids of TSC were loaded onto a Thermo Fisher Scientific Titan Krios transmission electron microscope equipped with a Gatan GIF Quantum energy filter (slit width 20 eV) and operating at 300 kV for data collection. All the cryo-EM images were automatically recorded by a post-GIF Gatan K2 Summit direct electron detector in the super-resolution counting mode using Serial-EM[49] with a nominal magnification of 105,000 x in the EFTEM mode, which yielded a super-resolution pixel size of 0.678 Å on the image plane, and with a defocus ranged from 1.0 to 3.5 μm. Each micrograph stack was dose-fractionated to 32 frames with a total electron dose of ~ 50 $e^-/ Å^2$ and a total exposure time of 11.49 s. For the first dataset of TSC sample, 3,316 micrographs from a total of 3,605 micrographs were selected for further processing. As for the second dataset of TSC sample, 1,381 micrographs from a total of 1,546 micrographs were selected for further processing.

Image processing. For cryo-EM data, drift and beam-induced motion correction were applied on the super-resolution movie stacks using MotionCor2[50] and binned two fold to a calibrated pixel size of 1.356 Å/pix. The defocus values were estimated by Gctf[51] from summed images without dose weighting. Other procedures of cryo-EM data processing were performed within RELION v3.0[52,53] using the dose-weighted micrographs.

For the first datasets of the TSC, a subset of ~ 10,000 particles were picked by Gautomatch (Zhang, unpublished) without reference and subjected to reference-free 2D classification. Some of the resulting 2D class averages were low-pass filtered to 15 Å and used as references for automatic particle picking of the whole datasets in RELION resulting in an initial set of 1,073,891 particles for reference-free 2D classification. 510,614 particles were selected from good 2D classes for the initial 3D classification, using a 60 Å low-pass filtered initial model from our previous cryo-EM reconstruction. After several rounds of 2D and 3D classification, 152,396 particles were 3D auto-refined and post-processed, yielding a reconstruction of TSC complex at 5.11 Å resolution. Also, for the second dataset of the TSC complex, a subset of ~ 10,000 particles were picked by Gautomatch (Zhang, unpublished) without reference and subjected to reference-free 2D classification. Some of the resulting 2D class averages were low-pass filtered to 20 Å and used as references for automatic particle picking of the whole datasets in RELION resulting in an initial set of 455,091 particles for reference-free 2D classification. 244,896 particles were selected from good 2D classes for the initial 3D classification, using a 60 Å low-pass filtered initial model from our previous cryo-EM reconstruction. After several rounds of 2D and 3D classification, 71,265 particles were 3D auto-refined and post-processed, yielding a reconstruction of TSC complex at 5.22 Å resolution. According to these reconstructions, $TSC^{dataset1}$ and $TSC^{dataset2}$ are the same sample. Thus, two datasets were merged to improve the map quality. After several rounds of 2D and 3D classification, 131,022 particles were 3D auto-refined and post-processed, yielding a reconstruction at 4.4 Å resolution. We used a local mask 3D refinement for the wing-a, core and wing-b region, 131,022 particles were local refined and post-processed, yielding a 4.1 Å reconstruction of TSC wing-a region, a 3.6 Å reconstruction of TSC core region, and a 3.9 Å reconstruction of TSC wing-b region, respectively.

All reported resolutions are based on the gold-standard Fourier shell correlation (FSC) = 0.143 criterion. The GSFSC curves were corrected for the effects of a soft mask with high-resolution noise substitution. All cryo-EM maps were sharpened by applying a negative B-factor estimated during post-processing in RELION. All the visualization and evaluation of the 3D volume map were performed within UCSF Chimera or UCSF ChimeraX[54], and the local resolution variations were calculated using RELION[52].

Model building and structure refinement. The cryo-EM maps of the TSC wing-a region complex at 4.1 Å resolution, the TSC core region complex at 3.6 Å resolution and the TSC wing-b region complex at 3.9 Å resolution were used for model fitting. The structures of TSC1-TBC1D7 (PDB: 5EJC) was used as initial structural templates, which were docked into the cryo-EM maps by rigid-body fitting using UCSF Chimera[54]. The structural models were further manually built *de novo* in COOT[55] and refined in real space using Phenix[56] with secondary structure and geometry restraints using the cryo-EM map. Overfitting of the model was monitored by refining the model in one of the two half maps from the gold-standard refinement approach and testing the refined model against the other map[57]. Statistics of the map reconstruction and model refinement can be found in Table 1. The final models were evaluated using MolProbity[58]. Map and model representations in the figures and movies were prepared by PyMOL (http://www.pymol.org*)*, UCSF Chimera or UCSF ChimeraX[59].

In vitro **GAP assay.** GTPase-activating activity was determined with a calorimetric assay[60] measuring the formation of inorganic phosphate. TSC complex (1 μM) and Rheb (3 μM) samples were added in buffer containing 25 mM Hepes (pH 7.4), 200 mM NaCL, 1 mM GTP in 50 μl reaction mixtures and incubated at 37° for 3 hours. Reactions were terminated by the addition of 100 μl of malachite green/acid molybdate solution. After 20 min of color development, OD620 was determined.

In vivo **GAP assay.** The 293A cells were transfected with Flag-S6K1, Flag-Rheb, Flag-TSC1, Myc-TBC1D7, Flag-TSC2 WT and mutants using PEI. After 48 h, the cells were collected and lysed for 30 min. The supernatant was collected by centrifuge and boiled with SDS loading buffer. The sample was conducted for western blotting. The primary antibody was incubated overnight and washed three times with TBST, and incubated with secondary antibody for 1 h. After extensive rinsing with TBST for three times, ECL was detected.

Declarations

Acknowledgments

We thank Center of Cryo-Electron Microscopy, Fudan University, Center of Cryo-Electron Microscopy, Peking University, Center for Biological Imaging of Institute of Biophysics (IBP) of Chinese Academy of Sciences, and National Center for Protein Science Shanghai (NCPSS) for the supports on cryo-EM data collection and data analyses.

This work was supported by grants from the National key R&D program of China (2016YFA0500700), the National Natural Science Foundation of China (31770781, 31830107, 31821002, 31425008), the Shanghai Municipal Science and Technology Major Project (2017SHZDZX01), Shanghai Municipal Science and Technology Commission (19JC1411500), the National Ten-Thousand Talent Program, the National Program for support of Top-Notch Young Professionals, and the Strategic Priority Research Program of the Chinese Academy of Sciences (grant no. XDB08000000).

Author Contributions

H. Y. prepared the samples for structural and biochemical analyses with help from X. C., J. L., H. Y., D. Y., and K. G.; Z. Y. performed EM analyses and model building with the help from N. L., J. C., and N. G.; Y. X. wrote the manuscript with the help from H. Y. and K. G.; Y. X. supervised the project.

Competing interests

Authors declare no competing interests.

Data and materials availability

Cryo-EM maps and atomic coordinates will be deposited upon acceptance of the manuscript.

References

1 Nojima, H. *et al.* The mammalian target of rapamycin (mTOR) partner, raptor, binds the mTOR substrates p70 S6 kinase and 4E-BP1 through their TOR signaling (TOS) motif. *J Biol Chem* **278**, 15461-15464, doi:10.1074/jbc.C200665200 (2003).

2 Saxton, R. A. & Sabatini, D. M. mTOR Signaling in Growth, Metabolism, and Disease. *Cell* **168**, 960-976, doi:10.1016/j.cell.2017.02.004 (2017).

3 Gai, Z. *et al.* Structure of the TBC1D7-TSC1 complex reveals that TBC1D7 stabilizes dimerization of the TSC1 C-terminal coiled coil region. *J Mol Cell Biol* **8**, 411-425, doi:10.1093/jmcb/mjw001 (2016).

4 Dibble, C. C. *et al.* TBC1D7 is a third subunit of the TSC1-TSC2 complex upstream of mTORC1. *Mol Cell* **47**, 535-546, doi:10.1016/j.molcel.2012.06.009 (2012).

5 van Slegtenhorst, M. *et al.* Interaction between hamartin and tuberin, the TSC1 and TSC2 gene products. *Hum Mol Genet* **7**, 1053-1057, doi:10.1093/hmg/7.6.1053 (1998).

6 Brownbridge, G. G., Lowe, P. N., Moore, K. J., Skinner, R. H. & Webb, M. R. Interaction of GTPase activating proteins (GAPs) with p21ras measured by a novel fluorescence anisotropy method. Essential role of Arg-903 of GAP in activation of GTP hydrolysis on p21ras. *J Biol Chem* **268**, 10914-10919 (1993).

7 Garami, A. *et al.* Insulin activation of Rheb, a mediator of mTOR/S6K/4E-BP signaling, is inhibited by TSC1 and 2. *Mol Cell* **11**, 1457-1466, doi:10.1016/s1097-2765(03)00220-x (2003).

8 Inoki, K., Li, Y., Xu, T. & Guan, K. L. Rheb GTPase is a direct target of TSC2 GAP activity and regulates mTOR signaling. *Genes & development* **17**, 1829-1834, doi:10.1101/gad.1110003 (2003).

9 Tee, A. R., Manning, B. D., Roux, P. P., Cantley, L. C. & Blenis, J. Tuberous sclerosis complex gene products, Tuberin and Hamartin, control mTOR signaling by acting as a GTPase-activating protein complex toward Rheb. *Curr Biol* **13**, 1259-1268, doi:10.1016/s0960-9822(03)00506-2 (2003).

10 Zhang, Y. *et al.* Rheb is a direct target of the tuberous sclerosis tumour suppressor proteins. *Nat Cell Biol* **5**, 578-581, doi:10.1038/ncb999 (2003).

11 Castro, A. F., Rebhun, J. F., Clark, G. J. & Quilliam, L. A. Rheb binds tuberous sclerosis complex 2 (TSC2) and promotes S6 kinase activation in a rapamycin- and farnesylation-dependent manner. *J Biol Chem* **278**, 32493-32496, doi:10.1074/jbc.C300226200 (2003).

12 Inoki, K., Corradetti, M. N. & Guan, K. L. Dysregulation of the TSC-mTOR pathway in human disease. *Nat Genet* **37**, 19-24, doi:10.1038/ng1494 (2005).

13 Henske, E. P., Jozwiak, S., Kingswood, J. C., Sampson, J. R. & Thiele, E. A. Tuberous sclerosis complex. *Nat Rev Dis Primers* **2**, 16035, doi:10.1038/nrdp.2016.35 (2016).

14 Qin, J. *et al.* Structural Basis of the Interaction between Tuberous Sclerosis Complex 1 (TSC1) and Tre2-Bub2-Cdc16 Domain Family Member 7 (TBC1D7). *J Biol Chem* **291**, 8591-8601, doi:10.1074/jbc.M115.701870 (2016).

15 Sun, W. *et al.* Crystal structure of the yeast TSC1 core domain and implications for tuberous sclerosis pathological mutations. *Nat Commun* **4**, 2135, doi:10.1038/ncomms3135 (2013).

16 Zech, R., Kiontke, S., Mueller, U., Oeckinghaus, A. & Kummel, D. Structure of the Tuberous Sclerosis Complex 2 (TSC2) N Terminus Provides Insight into Complex Assembly and Tuberous Sclerosis Pathogenesis. *J Biol Chem* **291**, 20008-20020, doi:10.1074/jbc.M116.732446 (2016).

17 Scrima, A., Thomas, C., Deaconescu, D. & Wittinghofer, A. The Rap-RapGAP complex: GTP hydrolysis without catalytic glutamine and arginine residues. *The EMBO journal* **27**, 1145-1153, doi:10.1038/emboj.2008.30 (2008).

18 Gao, X. & Pan, D. TSC1 and TSC2 tumor suppressors antagonize insulin signaling in cell growth. *Genes & development* **15**, 1383-1392, doi:10.1101/gad.901101 (2001).

19 Li, Y., Inoki, K. & Guan, K. L. Biochemical and functional characterizations of small GTPase Rheb and TSC2 GAP activity. *Mol Cell Biol* **24**, 7965-7975, doi:10.1128/MCB.24.18.7965-7975.2004 (2004).

20 Santiago Lima, A. J. *et al.* Identification of regions critical for the integrity of the TSC1-TSC2-TBC1D7 complex. *PLoS One* **9**, e93940, doi:10.1371/journal.pone.0093940 (2014).

21 Hoogeveen-Westerveld, M. *et al.* The TSC1-TSC2 complex consists of multiple TSC1 and TSC2 subunits. *BMC biochemistry* **13**, 18, doi:10.1186/1471-2091-13-18 (2012).

22 Yu, Y. *et al.* Structural basis for the unique biological function of small GTPase RHEB. *J Biol Chem* **280**, 17093-17100, doi:10.1074/jbc.M501253200 (2005).

23 Scheffzek, K. *et al.* The Ras-RasGAP complex: structural basis for GTPase activation and its loss in oncogenic Ras mutants. *Science* **277**, 333-338, doi:10.1126/science.277.5324.333 (1997).

24 Scheffzek, K. & Ahmadian, M. R. GTPase activating proteins: structural and functional insights 18 years after discovery. *Cell Mol Life Sci* **62**, 3014-3038, doi:10.1007/s00018-005-5136-x (2005).

25 Mishra, A. K. & Lambright, D. G. Invited review: Small GTPases and their GAPs. *Biopolymers* **105**, 431-448, doi:10.1002/bip.22833 (2016).

26 Mittal, R., Ahmadian, M. R., Goody, R. S. & Wittinghofer, A. Formation of a transition-state analog of the Ras GTPase reaction by Ras-GDP, tetrafluoroaluminate, and GTPase-activating proteins. *Science* **273**, 115-117, doi:10.1126/science.273.5271.115 (1996).

27 Daumke, O., Weyand, M., Chakrabarti, P. P., Vetter, I. R. & Wittinghofer, A. The GTPase-activating protein Rap1GAP uses a catalytic asparagine. *Nature* **429**, 197-201, doi:10.1038/nature02505 (2004).

28 Li, Y., Inoki, K., Vikis, H. & Guan, K. L. Measurements of TSC2 GAP activity toward Rheb. *Methods Enzymol* **407**, 46-54, doi:10.1016/S0076-6879(05)07005-9 (2006).

29 Marshall, C. B. *et al.* Characterization of the intrinsic and TSC2-GAP-regulated GTPase activity of Rheb by real-time NMR. *Sci Signal* **2**, ra3, doi:10.1126/scisignal.2000029 (2009).

30 Hansmann, P. *et al.* Structure of the TSC2 GAP Domain: Mechanistic Insight into Catalysis and Pathogenic Mutations. *Structure*, doi:10.1016/j.str.2020.05.008 (2020).

31 Tate, J. G. *et al.* COSMIC: the Catalogue Of Somatic Mutations In Cancer. *Nucleic Acids Res* **47**, D941-D947, doi:10.1093/nar/gky1015 (2019).

32 Inoki, K., Li, Y., Zhu, T., Wu, J. & Guan, K. L. TSC2 is phosphorylated and inhibited by Akt and suppresses mTOR signalling. *Nat Cell Biol* **4**, 648-657, doi:10.1038/ncb839 (2002).

33 Hodges, A. K. *et al.* Pathological mutations in TSC1 and TSC2 disrupt the interaction between hamartin and tuberin. *Hum Mol Genet* **10**, 2899-2905, doi:10.1093/hmg/10.25.2899 (2001).

34 Dufner Almeida, L. G. *et al.* Comparison of the functional and structural characteristics of rare TSC2 variants with clinical and genetic findings. *Hum Mutat* **41**, 759-773, doi:10.1002/humu.23963 (2020).

35 Hoogeveen-Westerveld, M. *et al.* Functional assessment of variants in the TSC1 and TSC2 genes identified in individuals with Tuberous Sclerosis Complex. *Hum Mutat* **32**, 424-435, doi:10.1002/humu.21451 (2011).

36 Nellist, M. *et al.* Distinct effects of single amino-acid changes to tuberin on the function of the tuberin-hamartin complex. *Eur J Hum Genet* **13**, 59-68, doi:10.1038/sj.ejhg.5201276 (2005).

37 Manning, B. D., Tee, A. R., Logsdon, M. N., Blenis, J. & Cantley, L. C. Identification of the tuberous sclerosis complex-2 tumor suppressor gene product tuberin as a target of the phosphoinositide 3-Kinase/Akt pathway. *Molecular Cell* **10**, 151-162, doi:Doi 10.1016/S1097-2765(02)00568-3 (2002).

38 Cai, S. L. *et al.* Activity of TSC2 is inhibited by AKT-mediated phosphorylation and membrane partitioning. *The Journal of cell biology* **173**, 279-289, doi:10.1083/jcb.200507119 (2006).

39 Inoki, K., Zhu, T. & Guan, K. L. TSC2 mediates cellular energy response to control cell growth and survival. *Cell* **115**, 577-590, doi:10.1016/s0092-8674(03)00929-2 (2003).

40 Li, Y., Inoki, K., Vacratsis, P. & Guan, K. L. The p38 and MK2 kinase cascade phosphorylates tuberin, the tuberous sclerosis 2 gene product, and enhances its interaction with 14-3-3. *J Biol Chem* **278**, 13663-

13671, doi:10.1074/jbc.M300862200 (2003).

41 Shumway, S. D., Li, Y. & Xiong, Y. 14-3-3beta binds to and negatively regulates the tuberous sclerosis complex 2 (TSC2) tumor suppressor gene product, tuberin. *J Biol Chem* **278**, 2089-2092, doi:10.1074/jbc.C200499200 (2003).

42 Demetriades, C., Plescher, M. & Teleman, A. A. Lysosomal recruitment of TSC2 is a universal response to cellular stress. *Nature communications* **7**, 10662, doi:10.1038/ncomms10662 (2016).

43 Su, Q. P. *et al.* Vesicle Size Regulates Nanotube Formation in the Cell. *Sci Rep* **6**, 24002, doi:10.1038/srep24002 (2016).

44 Menon, S. *et al.* Spatial Control of the TSC Complex Integrates Insulin and Nutrient Regulation of mTORC1 at the Lysosome. *Cell* **156**, 771-785, doi:10.1016/j.cell.2013.11.049 (2014).

45 Demetriades, C., Doumpas, N. & Teleman, A. A. Regulation of TORC1 in response to amino acid starvation via lysosomal recruitment of TSC2. *Cell* **156**, 786-799, doi:10.1016/j.cell.2014.01.024 (2014).

46 Dere, R., Wilson, P. D., Sandford, R. N. & Walker, C. L. Carboxy terminal tail of polycystin-1 regulates localization of TSC2 to repress mTOR. *PLoS One* **5**, e9239, doi:10.1371/journal.pone.0009239 (2010).

47 McLaughlin, S. & Murray, D. Plasma membrane phosphoinositide organization by protein electrostatics. *Nature* **438**, 605-611, doi:10.1038/nature04398 (2005).

48 Kastner, B. *et al.* GraFix: sample preparation for single-particle electron cryomicroscopy. *Nat Methods* **5**, 53-55, doi:10.1038/nmeth1139 (2008).

49 Mastronarde, D. N. Automated electron microscope tomography using robust prediction of specimen movements. *J Struct Biol* **152**, 36-51, doi:10.1016/j.jsb.2005.07.007 (2005).

50 Zheng, S. Q. *et al.* MotionCor2: anisotropic correction of beam-induced motion for improved cryo-electron microscopy. *Nat Methods* **14**, 331-332, doi:10.1038/nmeth.4193 (2017).

51 Zhang, K. Gctf: Real-time CTF determination and correction. *J Struct Biol* **193**, 1-12, doi:10.1016/j.jsb.2015.11.003 (2016).

52 Kimanius, D., Forsberg, B. O., Scheres, S. H. W. & Lindahl, E. Accelerated cryo-EM structure determination with parallelisation using GPUs in RELION-2. *Elife* **5**, doi:ARTN e18722 10.7554/eLife.18722 (2016).

53 Scheres, S. H. W. RELION: Implementation of a Bayesian approach to cryo-EM structure determination. *J Struct Biol* **180**, 519-530, doi:10.1016/j.jsb.2012.09.006 (2012).

54 Pettersen, E. F. *et al.* UCSF chimera - A visualization system for exploratory research and analysis. *J Comput Chem* **25**, 1605-1612, doi:10.1002/jcc.20084 (2004).

55 Emsley, P. & Cowtan, K. Coot: model-building tools for molecular graphics. *Acta Crystallogr D* **60**, 2126-2132, doi:10.1107/S0907444904019158 (2004).

56 Adams, P. D. *et al.* PHENIX: building new software for automated crystallographic structure determination. *Acta Crystallogr D* **58**, 1948-1954, doi:10.1107/S0907444902016657 (2002).

57 Amunts, A. *et al.* Structure of the Yeast Mitochondrial Large Ribosomal Subunit. *Science* **343**, 1485-1489, doi:10.1126/science.1249410 (2014).

58 Chen, V. B. *et al.* MolProbity: all-atom structure validation for macromolecular crystallography. *Acta Crystallogr D* **66**, 12-21, doi:10.1107/S0907444909042073 (2010).

59 Goddard, T. D. *et al.* UCSF ChimeraX: Meeting modern challenges in visualization and analysis. *Protein Sci* **27**, 14-25, doi:10.1002/pro.3235 (2018).

60 Cairns, B. R., Kim, Y. J., Sayre, M. H., Laurent, B. C. & Kornberg, R. D. A multisubunit complex containing the SWI1/ADR6, SWI2/SNF2, SWI3, SNF5, and SNF6 gene products isolated from yeast. *Proc Natl Acad Sci U S A* **91**, 1950-1954, doi:10.1073/pnas.91.5.1950 (1994).

Figures

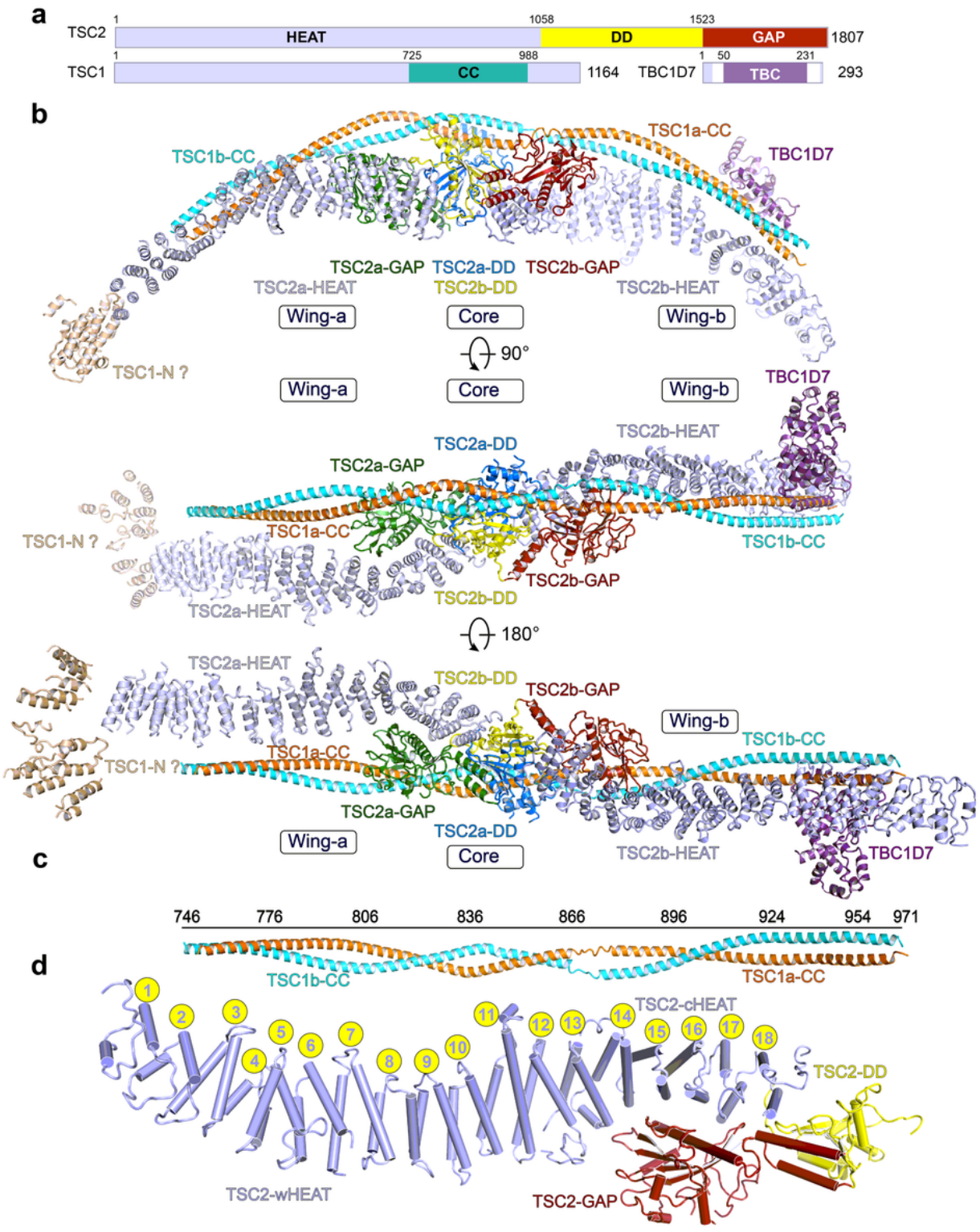

Figure 1

Overall structure of human TSC complex. a Color-coded domain structure of the three subunits with invisible regions colored in grey. Residues at domain boundaries are indicated with numbers. The same color scheme is used throughout all structure figures unless indicated elsewhere. HEAT, HEAT repeat domain; GAP, GTPase activating domain; CC: coiled-coil; DD, dimerization domain; TBC, Tre2-Bub2-Cdc16 domain. b Ribbon representation of TSC complex structure in three different views. The modules and

subunits are labeled and indicated. c TSC1 coiled-coil dimer structure with residue positions indicated. d Cartoon model of one of TSC2 monomer, the HEAT repeats are indicated with numbered balls.

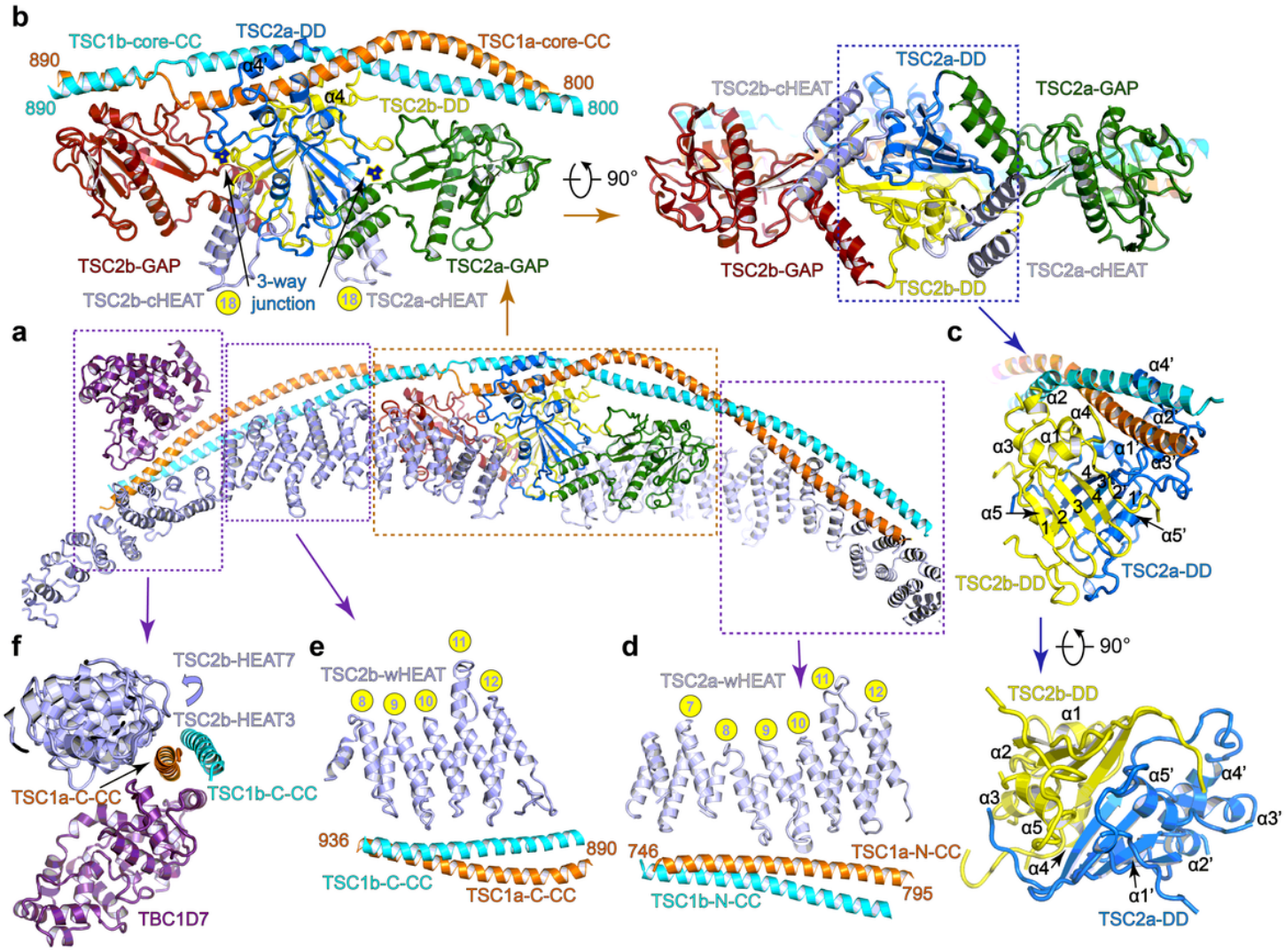

Figure 2

Intermolecular interfaces of TSC complex. a Overall structure of TSC complex shown in a view different from that in Fig. 1b, intermolecular contacts shown in b-f are highlighted with dashed boxes. b Close-up view of the intermodular interactions in the central core module. c-f, Close-up view of the intermodular interactions in the dimerization domain (c), wing-a (d), wing-b (e), and TSC1 C-CC with TBC1D7 (f). Critical elements are indicated. In (c), α1-α5 and α1'-α5' represent α helices of TSC2b and TSC2a, respectively. The numbers (1-4 and 1'-4') represent the numbered β strands.

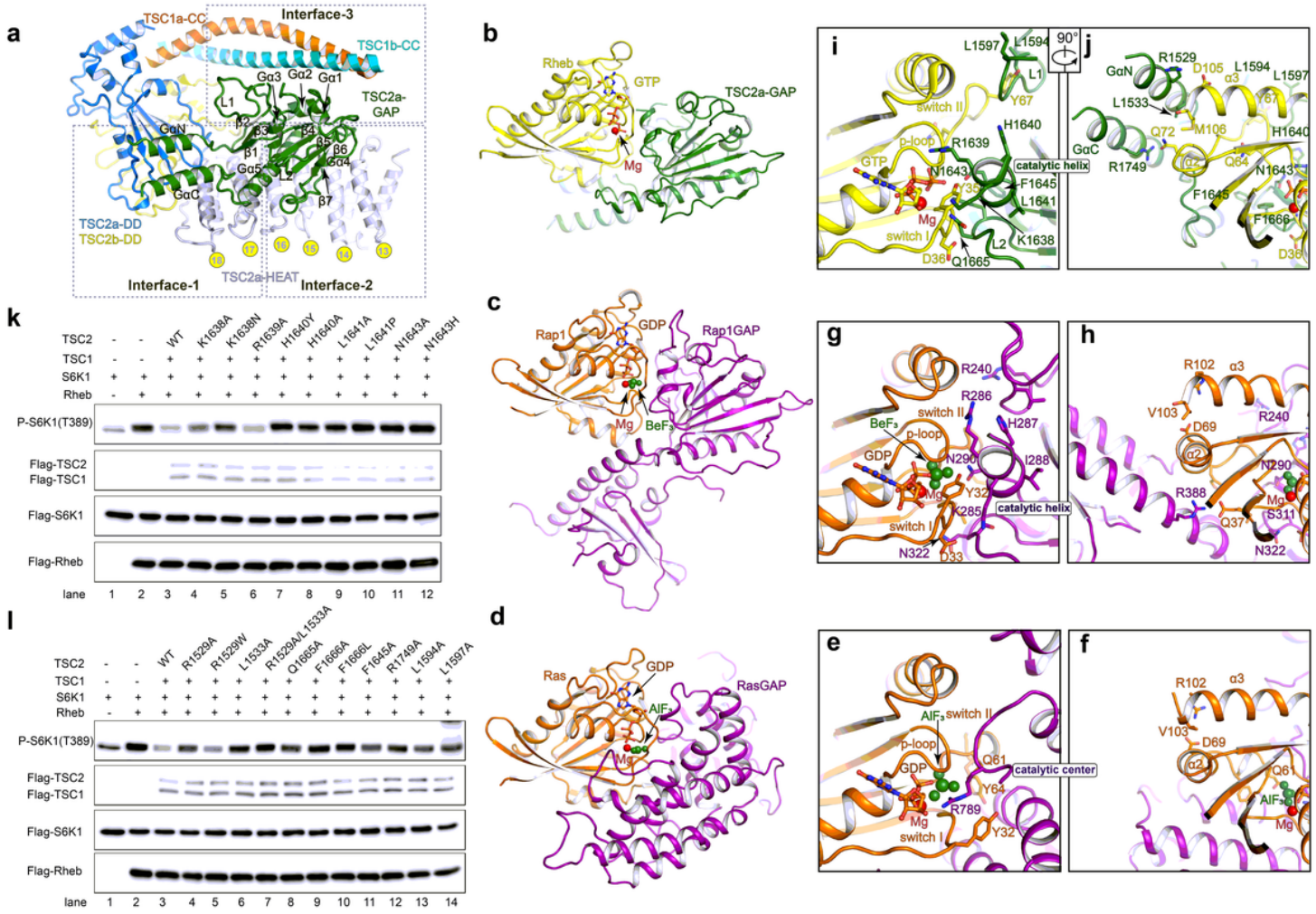

Figure 3

TSC2 GAP catalytic mechanism and putative GAP-Rheb binding. a Close-up view of TSC2a GAP domain and its positioning. Three inter-domain contacts are highlighted with dashed boxes. b-d, Structural comparison of Rheb-TSC2 GAP (b), Rap1-Rap1GAP (PDB:3BRW) (c), and Ras-RasGAP (PDB:1WQ1) (d). The structures are shown in a similar view. TSC2 GAP and Rheb are shown in green and yellow, respectively. Rap1 and Ras are colored in orange and Rap1GAP and RasGAP are colored in magenta, respectively. In (b), the GTP-bound Rheb (PDB:1XTS) and TSC2 GAP domain were respectively superimposed to Rap1 and Rap1GAP in Rap1-Rap1GAP structure. e-i, Two different close-up views of the catalytic centers of RasGAP (e-f), Rap1GAP (g-h), and TSC2 (i-j). The structures are derived from Figure 3b-d. Magnesium cations are shown as red balls. The Beryllium trifluoride (BeF3) and Aluminum trifluoride (AlF3) are shown as green balls. The GDP-BeF3 and GDP-AlF3 is the mimetic ATP in ground and transition states, respectively. Residues involved in binding and catalysis are shown in sticks. k-l, Cell-base GAP activity assays of wild type TSC2 and TSC2 mutants. The activities were detected by western blotting with antibody against phosphorylated S6K (T389). The effects of residues involved in catalysis (k) and Rheb-binding (l) were tested.

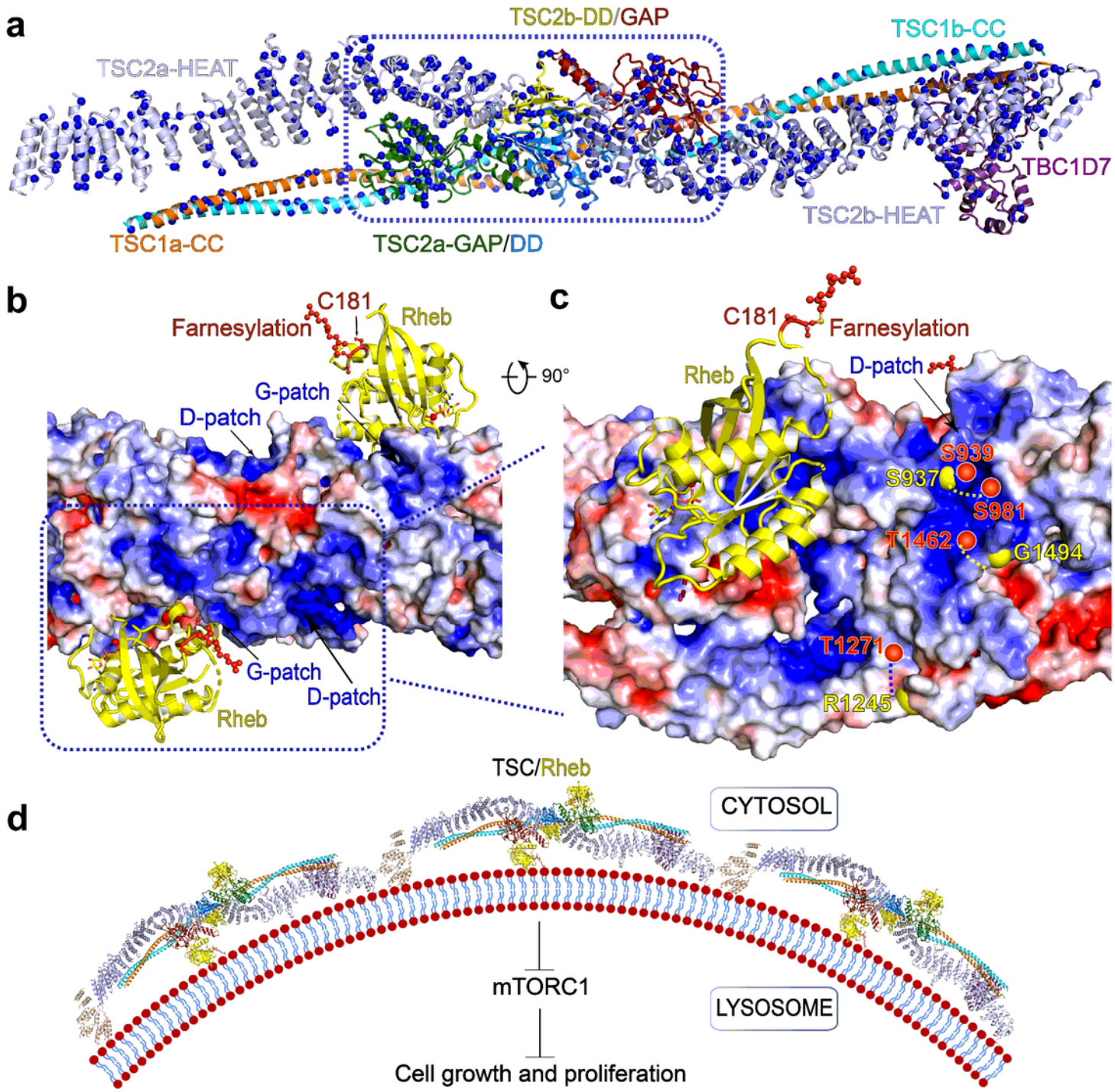

Figure 4

TSC Surface feature and functional implications. a The cartoon structure of TSC complex are shown with cancer-associated mutations highlighted with blue balls. b-c, Electrostatic potential surface of TSC complex is shown in two views. Two putative Rheb molecules (yellow) are shown in cartoon with farnesylation at C181 (red) indicated (b). Representative phosphorylation sites of TSC2 are projected onto the surface (red balls) with the nearest modeled residues (S937, R1245 and G1494) shown in yellow

balls. The positively charged patches around dimerization domain (D-patch) and GAP domain (G-patch) are shown in a close-up view. d A schematic model of TSC/Rheb localization on lysosomal membrane to regulate mTORC1 activity. The characteristic TSC architecture may fit the curved lysosomal surface.

Supplementary Files

This is a list of supplementary files associated with this preprint. Click to download.

- Supplementarymaterials.docx